

## Electronic Supplementary Information

### Single-imprint Moth-eye Anti-Reflective and Photoinduced Self-cleaning Film with Enhanced Resistance

Iván Navarro-Baena<sup>‡</sup>, Alejandra Jacobo-Martín<sup>‡</sup>, Jaime J. Hernández<sup>‡</sup>, Jose R. Castro Smirnov<sup>‡</sup>, Felipe Viela<sup>‡</sup>, Miguel A. Monclús<sup>§</sup>, Manuel R. Osorio<sup>‡</sup>, Jon M. Molina-Aldareguia<sup>§</sup>, Isabel Rodríguez<sup>‡\*</sup>

<sup>‡</sup>Madrid Institute for Advanced Studies in Nanoscience (IMDEA Nanoscience),  
C/ Faraday 9, Ciudad Universitaria de, Cantoblanco. 28049 Madrid, Spain  
*Iván Navarro-Baena, Jaime J. Hernández, Alejandra Jacobo-Martín, Jose R. Castro Smirnov,  
Felipe Viela, Manuel R. Osorio and Isabel Rodríguez*

<sup>§</sup>Madrid Institute for Advanced Studies in Materials (IMDEA Materials),  
C/ Eric Kandel, 2, Tecnogetafe, Getafe. 28906 Madrid, Spain  
*Miguel A. Monclús, Jon M. Molina-Aldareguia*

*\*Correspondence to: i.rodriguez@imdea.org*

## Characterization of synthesized Titania nanoparticles

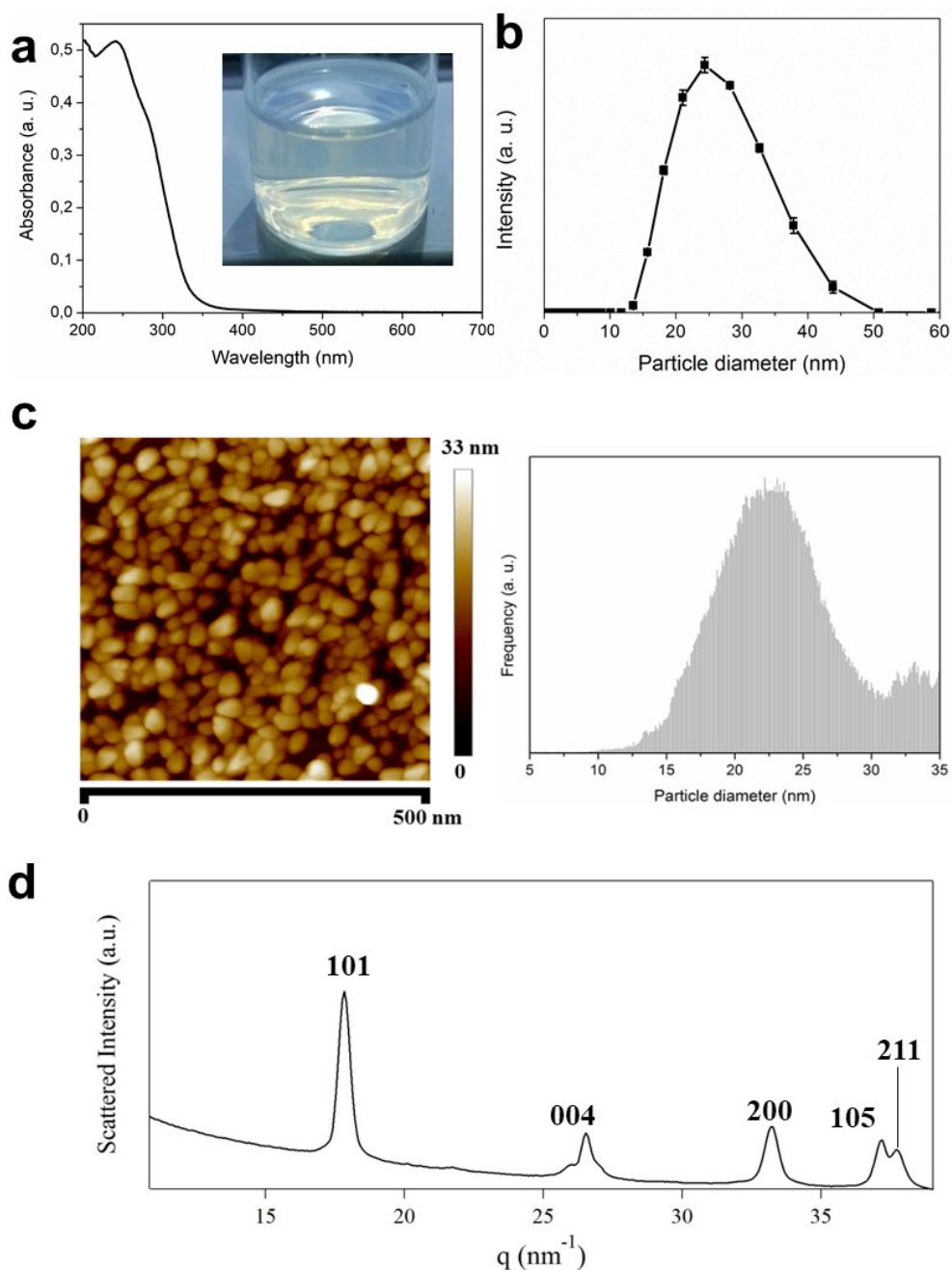


Figure S1: TiO<sub>2</sub> nanoparticle characterization: (a) Absorbance spectrum for synthesized TiO<sub>2</sub> nanoparticles and digital photograph of colloidal nanoparticles dispersion. (b) Dynamic light scattering size measurements. (c) AFM image of TiO<sub>2</sub> layered nanoparticles (1 wt %) prior imprinting. (d) 1D intensity WAXD profiles derived from the radial integration of the 2D diffraction patterns. The Miller indices of the main reflections are indicated.

Table S1: Structural parameters of TiO<sub>2</sub> –anatase derived from the WAXD measurements.

hkl	d <sub>obs</sub> (Å)	d <sub>calc</sub> (Å)
101	3.52	3.52
004	2.40	2.43
200	1.89	1.89
105	1.69	1.70
211	1.67	1.67

### Characterization of PMMA pre-printed surface

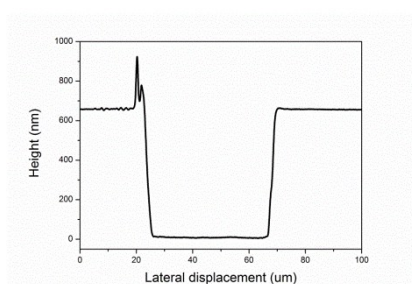


Figure S2. Profile of PMMA coating over PET

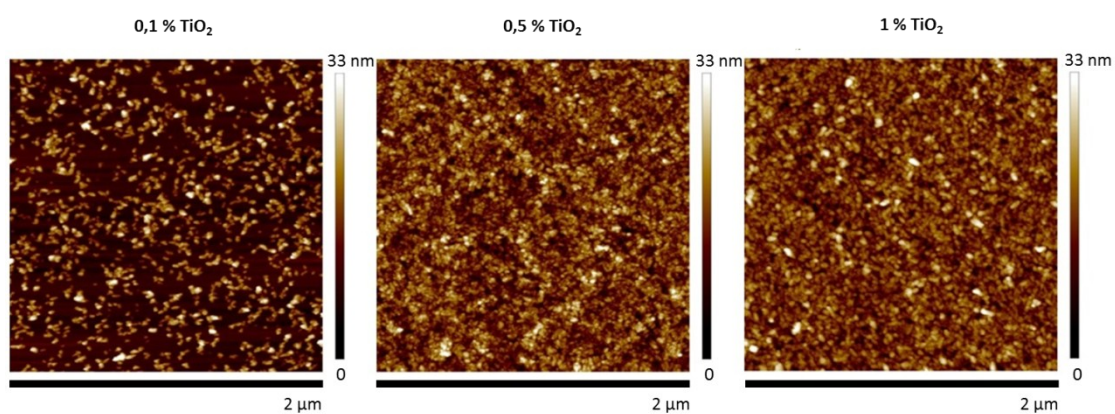


Figure S3. Morphological characterization of TiO<sub>2</sub> layer prior to imprinting.

## Morphological characterization of the moth-eye AR nanoimprinted films

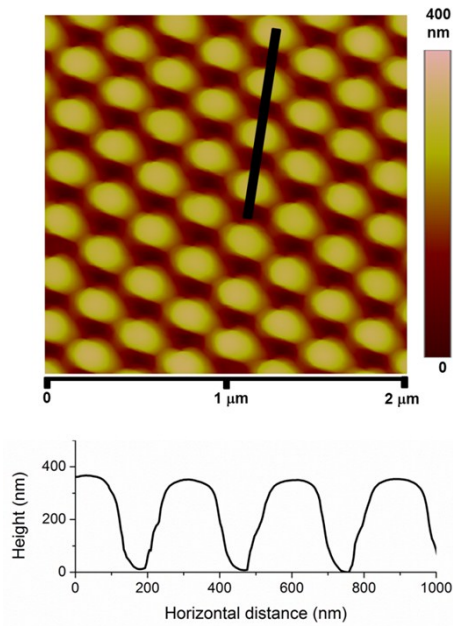


Figure S4: AFM height image of a P-AR substrate and cross-section profile corresponding to the black line.

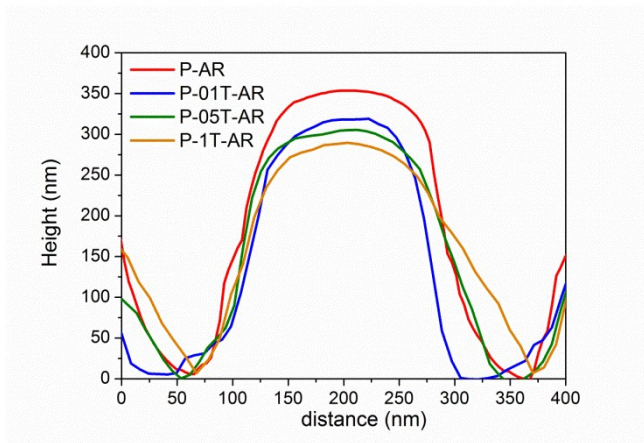


Figure S5. AFM profiles of a single moth-eye cone corresponding to the different TiO<sub>2</sub> composites tested.

Table S2: Morphologic parameters obtained from AFM measurements for the different TiO<sub>2</sub> composite AR surfaces.

Sample	Pitch (nm)	Depth (nm)	Peak top width (nm)	Aspect ratio
P-AR	250±2	340±15	115±15	2.9
P-01T-AR	252±4	320±15	118±12	2.7
P-05T-AR	255±3	290±30	122±13	2.4
P-1T-AR	255±2	270±20	120±13	2.3

## Extended transmission and reflection spectra

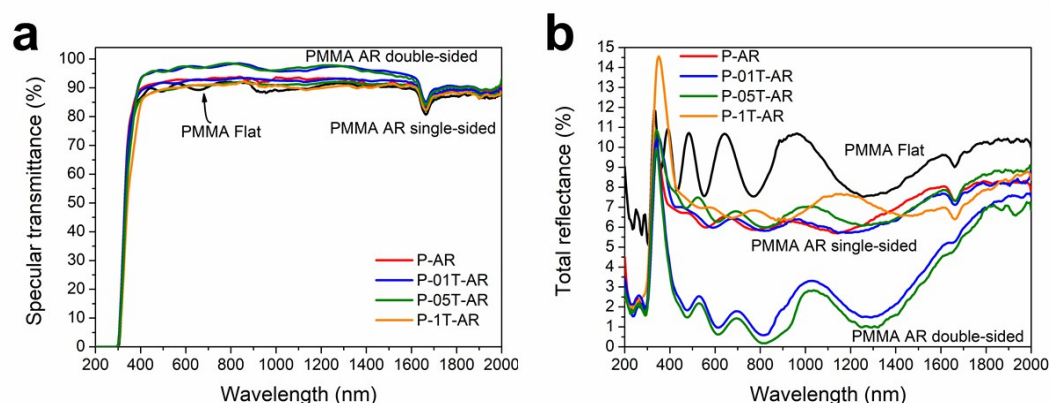


Figure S6. Extended transmission and reflection spectra of the moth-eye imprinted nanocomposite surfaces (200-2000 nm). a) Specular transmission spectra. b) Total reflection spectra.

## Scattering losses due to the moth-eye nanostructured surface

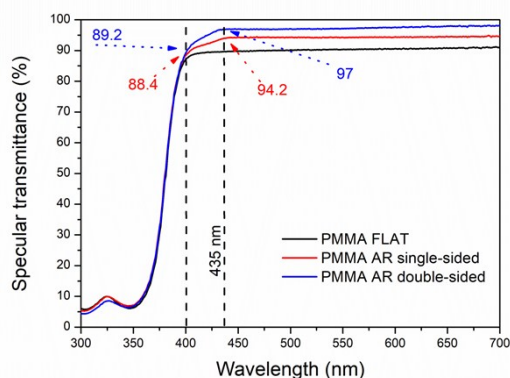


Figure S7. Reduction in transmittance due to scattering losses caused by the moth-eye topography. The spectra compares PMMA free standing films with a flat pristine surface, a film patterned on one side and with both sides patterned.

## Photocatalytic experiments on flat and imprinted surfaces

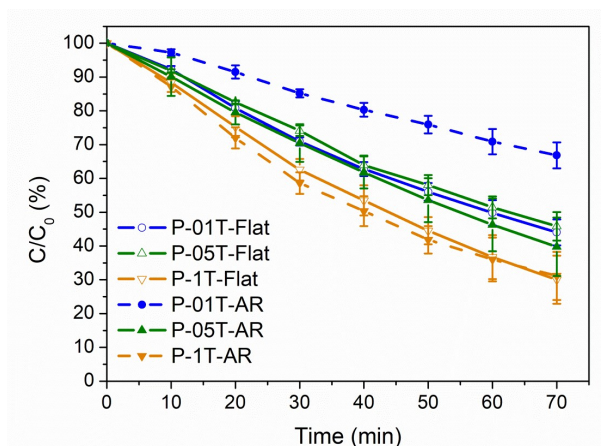


Figure S8. Comparison of photocatalytic activity between imprinted and non-imprinted samples with equal  $\text{TiO}_2$  load.

## Hydrophobicity recovery of the irradiated substrates

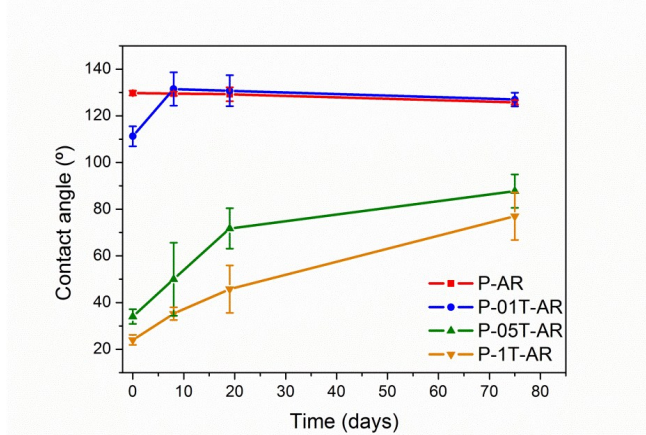


Figure S9. Hydrophobicity recovery of the UV irradiated substrates in wet conditions after a period of storage at room temperature in dry conditions.

## Weathering resistance of UV irradiated AR films

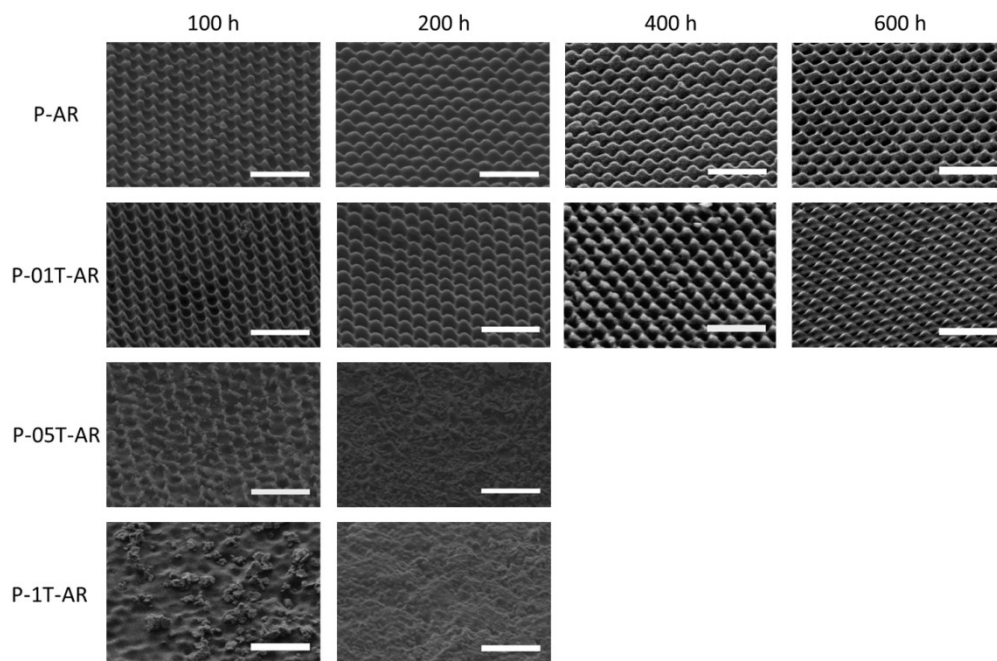


Figure S10. SEM images after the accelerated weathering tests. It can be observed that the moth-eye topography of the P-01T-AR substrate remained after 600h of exposure. However, the P-05T-AR and P-1T-AR substrates suffered substantial photo-degradation after 100 h of exposure. Scale bars correspond to 1 micron.

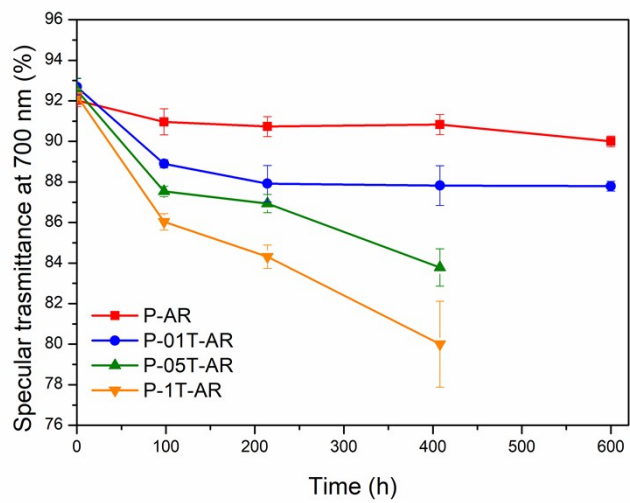


Figure S11. Optical transmittance variation as function of weathering time

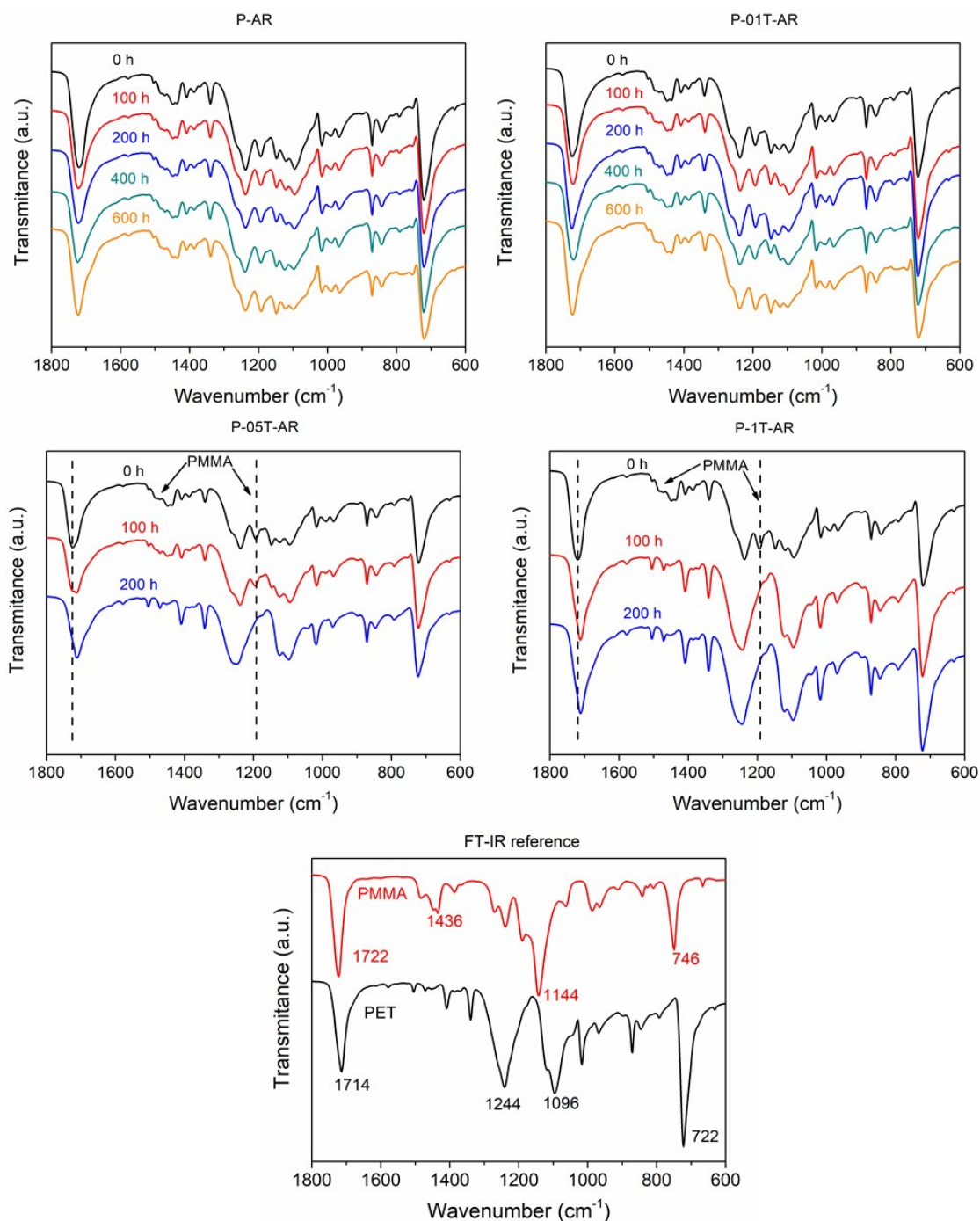


Figure S12. FTIR-ATR of moth-eye imprinted substrates measured before and after the accelerated weathering defined cycles. Due to the penetration depth of this technique, at the initial time, the characteristic peaks of PET and PMMA are seen in all substrates. The carbonyl peak of both polymers appears at  $1722\text{ cm}^{-1}$  for PMMA and at  $1714\text{ cm}^{-1}$  for PET. Hence, for monitoring the changes in chemical composition after withering conditions, the band at  $1144\text{ cm}^{-1}$ , which correspond to a C-O-C stretching vibration of PMMA, was compared on the different spectra obtained at 100, 200, 400, and 600h of weathering. P-AR and P-01T-AR did not show appreciable chemical changes even after 600 h of weathering. In contrast, the samples with higher nanoparticle load (P-05T-AR, P-1T-AR) show a clear reduction of the PMMA band, indicating the degradation of the PMMA matrix due to photo oxidation reactions taking place at accelerated conditions of radiation, heat and humidity.

## Mechanical characterization by nanoindentation and nanoscratch tests

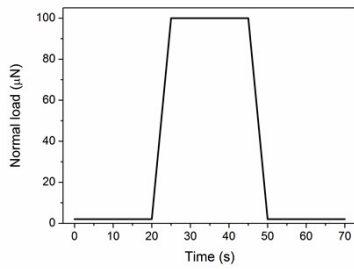


Figure S13. Representative load profile corresponding to a scratch test

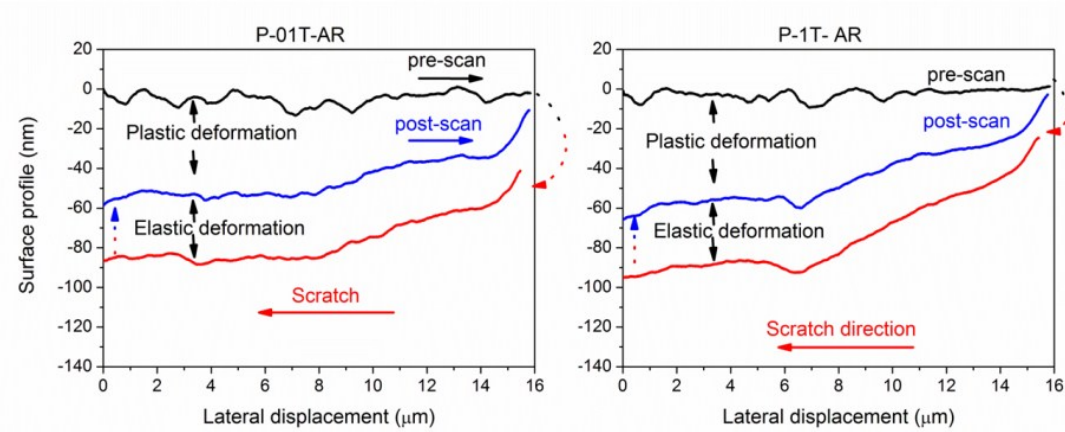
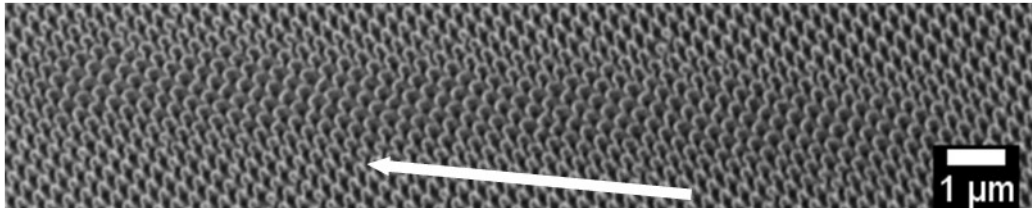


Figure S14. Normal scratch displacement profiles on P-01T-AR and on P-1T-AR substrates upon application of a constant normal force of 100  $\mu\text{N}$ .

### P-AR



### P-1T-AR

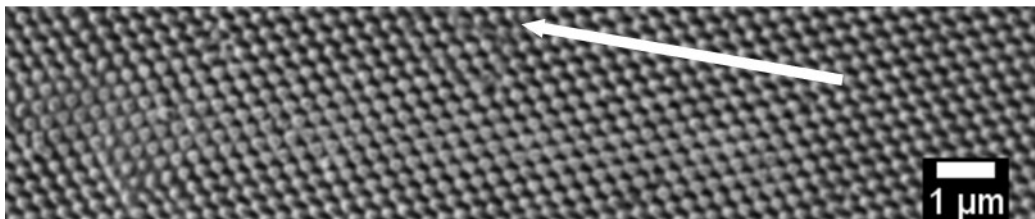


Figure S15. Scratch marks after nanoscratch tests on a P-AR and P-1T-AR substrates using a constant normal force of 100  $\mu\text{N}$ . The nanocones display plastic deformation in the scratch direction (indicated by the white arrow).